Assessment of GNSS stations using atmospheric horizontal gradients and microwave radiometry

Available online at www.sciencedirect.com

ScienceDirect

Advances in Space Research xxx (xxxx) xxx

ADVANCES IN SPACE RESEARCH (a COSPAR publication)

www.elsevier.com/locate/asr

Assessment of GNSS stations using atmospheric horizontal gradients and microwave radiometry

Gunnar Elgered [a,*], Tong Ning [b], Periklis-Konstantinos Diamantidis [a], Tobias Nilsson [b]

[a] Chalmers University of Technology, Onsala Space Observatory, SE-439 92 Onsala, Sweden
[b] Lantmäteriet (Swedish Mapping, Cadastral and Land Registration Authority), SE-801 82 Gävle, Sweden

Received 13 January 2023; received in revised form 2 May 2023; accepted 5 May 2023

Abstract

We have assessed the quality of four co-located GNSS stations by studying time series of estimated linear horizontal gradients in the signal delay. The stations have different electromagnetic environments. We also examine the consistency of the results by using two different GNSS softwares, GipsyX and c5++, and applying three different elevation cutoff angles: 5°, 10°, and 20°. The estimated gradients are compared with the corresponding ones estimated from microwave radiometer observations acquired during six months (April–September 2021). For all four stations and using both softwares we find that is is possible to track gradient variations over time scales from less than one hour using GPS observations only. We have indications that it is an advantage to equip the area below the GNSS antenna with microwave absorbing material. However, the differences are small, a reduction in rms differences in the gradients compared to those from the microwave radiometer of less than 2 %. More studies are needed to decide if such an investment is reasonable in terms of cost and maintenance.

Keywords: GNSS; Microwave radiometry; Water vapour; Horizontal gradients

1. Introduction

Data acquired from ground-based continuously operating Global Navigation Satellite Systems (GNSS) stations are used in various applications. For example, networks of GNSS receivers provide three-dimensional measurements of the movements in the Earth crust which are used to constrain models of the glacial isostatic adjustment process in Fennoscandia (Lidberg et al., 2010; Kierulf et al., 2021). A meteorological application is the use of equivalent Zenith Total Delays (ZTD) in a state-of-the-art km-scale numerical weather prediction (Lindskog et al., 2017). GNSS networks are also used to monitor the long-term changes in the water vapour content (Chen and Liu, 2016; Parracho et al., 2018). The focus of this study is on estimated linear horizontal gradients. Several applications related to the use of these gradients in meteorology have been reported. For example, a study of a hurricane (Graffigna et al., 2019), assessment of their impact in variational data assimilation (Zus et al., 2019), and gradients in coastal areas with a steep topography (Morel et al., 2015). In difference to geodesy, where parameters such as station positions often are estimated once per day, a significantly higher temporal resolution is of benefit for meteorological studies.

Although the existence of multipath is exploited in some remote sensing applications, e.g., monitoring of the sea level (Geremia-Nievinski et al., 2020) and the snow depth (Schmid et al., 2015), it is in general an unwanted effect when estimating geodetic and atmospheric parameters. The impact of multipath may be viewed as an extra signal

* Corresponding author.
E-mail address: Gunnar.Elgered@chalmers.se (G. Elgered).

https://doi.org/10.1016/j.asr.2023.05.010
0273-1177/

delay, depending on the azimuth and elevation angles of the observation, compared to the direct propagation path. Even if the electromagnetic environment causing the multipath is stable, the estimated parameters are affected at the absolute level. Estimated horizontal atmospheric gradients are especially sensitive to multipath, given that the effect is likely to depend on the azimuth angle. Impacts on the ZTD and on the horizontal gradients, may be assessed by applying different elevation cutoff angles in the GNSS data processing (Elgered et al., 2019; Ning and Elgered, 2021).

We used four co-located GNSS stations, of different designs (see Fig. 1), to estimate the ZTD and linear horizontal gradients as well as coordinates in the east, the north, and the vertical directions. The gradient time series are compared with each other and with those from a microwave radiometer sensitive to atmospheric water vapour. In this application it is often referred to as a Water Vapour Radiometer (WVR).

It is important to note that in spite of the fact that significant horizontal gradients exist now and then the assumption of linear gradients is rather crude. Examples of weather phenomena that will cause horizontal gradients in water vapour are sea breeze (Craig et al., 1945; Miller et al., 2003) and cloud rolls (Kuettner, 1971). We also note that water vapour may vary significantly over short time scales which in combination with the crude linear model imply that for comparisons using different instruments and methods synchronisation of the observations in space (the direction on the sky) and time is important. Furthermore, it is difficult to assess the quality of gradients estimated with a high temporal resolution simply because there are no independent results of superior accuracy available. Numerical weather models are useful to evaluate GNSS estimated gradients for a temporal resolution of hours, especially when assessing the consistency between gradients estimated for many stations in a region (Kačmařík et al., 2019). For applications with a higher temporal resolution it is possible to use a WVR, which has an accuracy similar to that of GNSS. Although this method suffers from poor accuracy during rain and when clouds containing large water drops are presented, it can provide independent wet delays in different directions on the sky.

The specifications of the GNSS stations and the WVR are described in Section 2 together with the corresponding data processing. In Section 3 we first summarise the gradient results of the four time series from the GNSS stations with each other. Thereafter we focus on the gradients obtained from the GNSS stations relative to the ones obtained from the WVR. We discuss the results and the possible consequences in Section 4. Finally, the conclusions are given in Section 5.

2. Instrumentation and data

2.1. GNSS stations

The Swedish GNSS network of permanent reference stations, SWEPOS^{TM}, is operated by Lantmäteriet (Swedish Mapping, Cadastral and Land Registration Authority). Currently (January 2023) the SWEPOS network consists of 478 permanent reference sites where 21 concrete pillar stations serve as the backbone for SWEREF 99 (the national reference frame). To keep the time series of the 21 fundamental stations consistent, the antennas of these pillar stations are not to be changed as long as they work properly. Thus, most of these stations have old antennas which have problems tracking some of the newer GNSS signals, such as Galileo and GPS L5, properly. In order to track also those signals, a steel truss mast was installed closely to each pillar with a newer antenna model (LEIAR25.R3) and a radome (LEIT). It is therefore of interest to investigate the performance of these different designs.

The main characteristics of four GNSS stations selected for the study are summarised in Table 1 and their locations are seen in Fig. 2. The station ONSA is one of the 21 fundamental stations of the SWEPOS network, but with a 1 m concrete pillar instead of the standard 3 m pillar. ONSA is also equipped with a microwave absorbing plate (610 ×

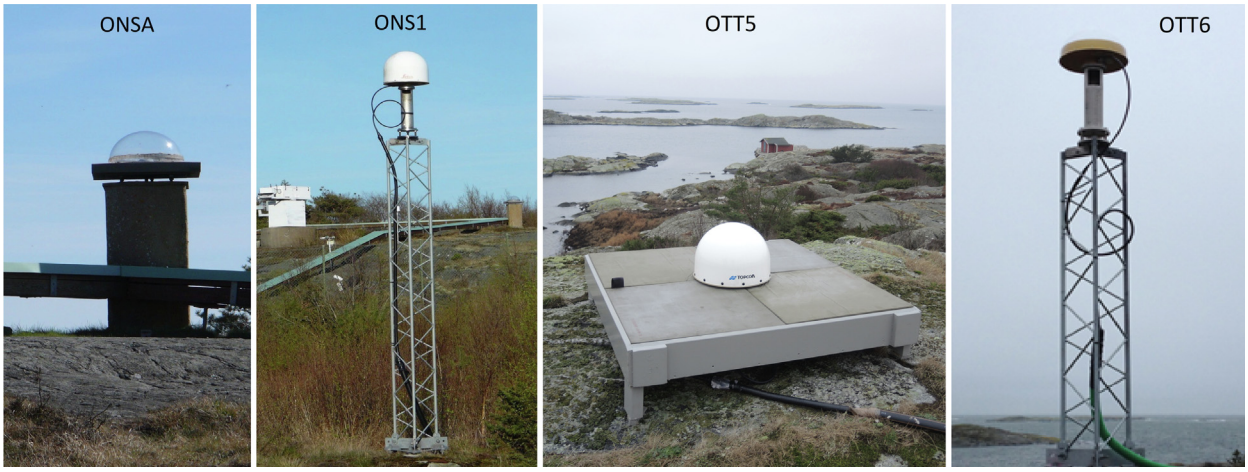

Fig. 1. The four GNSS stations (from left to right) are ONSA, ONS1, OTT5, and OTT6.

Table 1
GNSS stations at the Onsala site.

Station	Antenna	Radome	Receiver	Pillar	Height [m]	Distance[a] [m]
ONSA	AOADM/M_B	OSOD	SEPT POLARX5TR	1 m concrete	46.6	11
ONS1	LEIAR25.R3	LEIT	TRIMBLE ALLOY	3 m steel	44.5	54
OTT5	TPSCR.G5	TPSH	JAVAD TRE_G3T SIGMA	None	48.8	420
OTT6	JAVRINGANT_DM	OSOS	JAVAD TRE_G3T SIGMA	2 m steel	47.3	474

[a] The distance from the location of the WVR.

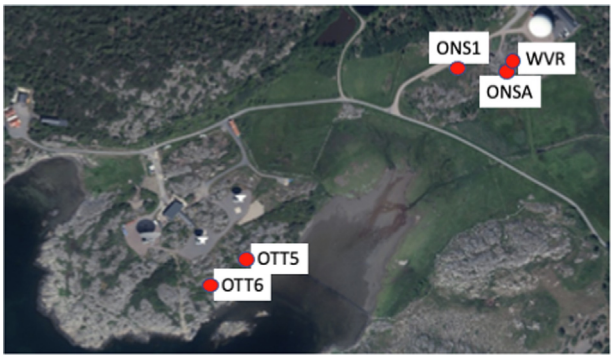

Fig. 2. The locations of the four GNSS stations and the WVR.

610 × 57 mm) below the antenna. ONS1 is one of the 21 secondary stations which are installed close to each concrete pillar and has a 3 m truss mast. The OTT5 station is made significantly different from the others. The antenna is mounted directly above the bedrock with a larger plate (1220 × 1220 × 114 mm) of microwave absorbing material below. OTT6 has an installation similar to ONS1 but the truss mast has a height equal to 2 m. All four GNSS stations have hemispheric radomes. It has been shown that a hemispheric radome design is preferred in order to minimize errors in the estimated ZWD and coordinates, see e.g., Emardson et al. (2000) and Ning et al. (2011).

We used two different analysis packages to process the data: GipsyX (Bertiger et al., 2020) and c5++ (Hobiger et al., 2010). See Table 2 for a summary of the setup. First we noticed that the four stations produced a different number of observations from the different GNSS. After a more detailed investigation we noted that the receivers at OTT5 and OTT6 had significantly less observations from Glonass and Galileo compared with ONSA and ONS1. Therefore, in order to make a more fair comparison in terms of the quality of the stations, only GPS observations were used in the assessment. The geometry of the observations are important for the estimated horizontal gradients. Fig. 3 shows examples of satellite positions on the sky. The figure is representative for the GipsyX processing using a sample period of 30 s. For the c5++ processing a sample period of 5 min was used. The reason for decimating the GPS data in c5++ is to obtain meaningful uncertainties, see e.g. Petovello et al. (2009).

Regarding the setup of the processing we note that some parameters have a significant impact on the estimated gradients, such as the gradient mapping function (Kačmařík et al., 2019) and including 2nd order ionospheric effects (Zus et al., 2017). However, we have made no attempt to have identical setup of GipsyX and c5++ because our task is to compare the gradients from four GNSS stations, and this is done independently for each software.

2.2. The water vapour radiometer Konrad

The microwave radiometer, shown in Fig. 4, was designed in order to provide independent estimates of the wet propagation delays for space geodetic applications. It measures the emission from the sky, on and off the water vapour line at 22.2 GHz. Its specifications are summarised in Table 3 and the data processing was carried out as described by Elgered et al. (2019) and references therein.

During the time April–September 2021 the WVR was observing in a sky mapping mode as is illustrated in Fig. 5. A disadvantage of a WVR is that the algorithm for calculation of the wet propagation delay fails for data acquired during rain, or when large liquid drops are presented in the sensed atmosphere. Typically such conditions imply large positive errors in the wet delay, and the water vapour content (Westwater and Guiraud, 1980). Therefore, data taken during rain, or when the estimated equivalent amount of liquid water in the zenith direction was $>$ 0.7 mm, were discarded from the gradient analysis.

The WVR is sensitive to the wet gradients only, whereas the estimates from the GPS processing result in total gradients. Therefore, the so called hydrostatic gradient must be added to the wet gradients before the comparison. The ERA5 reanalysis from the European Centre for Medium-Range Weather Forecasts (ECMWF) was used to calculate the hydrostatic gradients, in the east and the north directions, to generate total gradients based on the radiometer observations. We added VMF3-referred horizontal hydrostatic gradients (re3data.org, 2020) based on the ERA5 numerical weather model data to the WVR-derived gradients.

3. Results

3.1. GPS gradients vs GPS gradients

First we compare the gradient time series from the four GNSS stations against each other. Here we expect a relatively good agreement because the sampling of the

Table 2
Summary of GPS data processing.

Parameter	GipsyX v2.0	c5++
GNSS data	GPS only	
Strategy	Precise Point Positioning	
Clock and orbit parameters	JPL[a]	CODE (Dach et al., 2021)
Sample period	30 s	5 min
Ambiguity resolution	Yes	Yes (float)
Mapping function	VMF1, (Boehm et al., 2006)	VMF3, (Landskron and Bohm, 2018)
Gradient mapping function	(Bar-Sever et al., 1998)	(Chen and Herring, 1997)
Elevation cutoff angle	5°, 10°, 20°	
Weighting	No	Elevation-dependent[b]
Antenna PCV	igs14_2136.atx (Schmid et al., 2007)	
ZTD every 5 min	10 mm$\sqrt{\text{h}}^{-1}$	6 mm$\sqrt{\text{h}}^{-1}$
Gradient every 5 min	0.3 mm$\sqrt{\text{h}}^{-1}$	0.6 mm$\sqrt{\text{h}}^{-1}$
Ionosphere model	2nd order (IGRF)[c] (Matteo and Morton, 2011).	
Ocean tide loading	FES2004 (Lyard et al., 2006)	

[a] https://sideshow.jpl.nasa.gov/pub/JPL_GPS_Products/readme.txt.
[b] Coupled with variance component estimation of the Helmert type.
[c] International Geomagnetic Reference Field

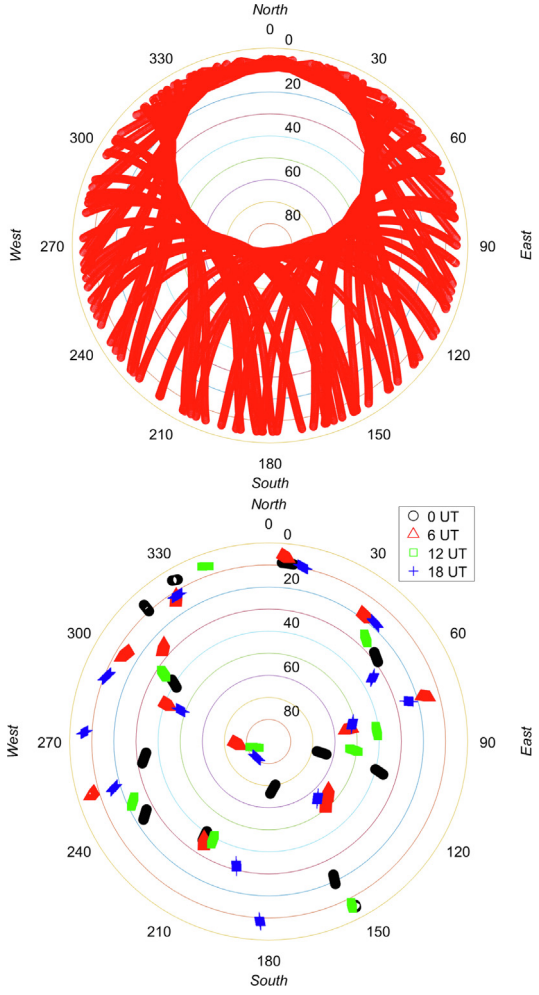

Fig. 3. Sky map of GPS satellites visible from Onsala during 24 h on 1 April, 2021 (top). The satellites visible at 5 min periods (10 samples used in the GipsyX processing) at 0, 6, 12, and 18 UT (bottom). Each 30 s sample is plotted with one symbol.

Fig. 4. The water vapour radiometer (WVR) Konrad.

atmosphere is similar for the four stations and they also share several common error sources. The results from the pairwise comparison are shown in Table 4. Here we have synchronised the four time series to use the same time epochs resulting in 51,839 and 52,311 data points in each time series for the GipsyX and the c5++ software, respectively. The original 5 min resolution for the gradient estimates and a 5° elevation cutoff angle were used. The GipsyX gradients show a significantly better agreement compared with the time series from c5++. This is expected because of the looser constraint applied in the gradient estimation process and the sample period of 5 min, resulting in less observations which is important when the temporal resolution is 5 min. In the following we therefore focus on the GipsyX results but include c5++ results in some specific comparisons when we regard them as meaningful.

Table 3
Specifications for the Konrad WVR.

Parameter	Value
Frequencies, channel 1/ channel 2	20.6 GHz/ 31.6 GHz
Antenna type (one for each channel)	Conical horn with lens
Antenna beam FWHM[a], E-plane, channel 1/ channel 2	2.9°/ 2.0°
Antenna beam FWHM[a], H-plane, channel 1/ channel 2	3.4°/ 2.3°
Reference temperatures (both channels)	313 and 373 K
System noise temperatures, channel 1/ channel 2	450/ 550 K
RF bandwidth (double sideband, both channels)	320 MHz
Absolute accuracy (weather dependent due to the quality of tip curves)	1–3 K
Repeatability	0.1 K

[a] FWHM = Full Width Half Maximum.

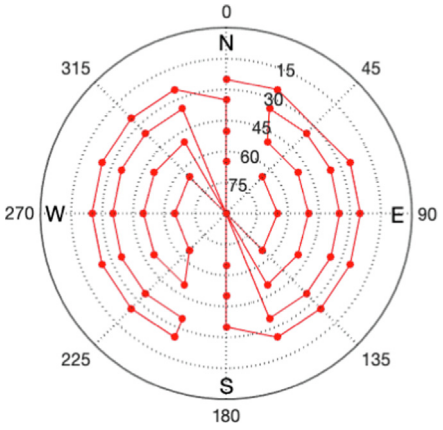

Fig. 5. The measurement cycle of the WVR. In order to avoid emission from the ground the lowest elevation angle (the centre of the antenna beam) observed was 25°. A cycle consists of 52 observations that starts in the north at an elevation angle of 25°. The cycle is 5 min long and was repeated continuously.

Table 4
Correlation coefficients (upper right triangle) and standard deviations in mm (lower left triangle) for gradient time series from the four GNSS stations using a 5° elevation cutoff angle.

Station	ONSA	ONS1	OTT5	OTT6
East gradient, GipsyX				
ONSA	–	0.92	0.94	0.94
ONS1	0.25	–	0.91	0.92
OTT5	0.20	0.27	–	0.94
OTT6	0.21	0.26	0.22	–
East gradient, c5++				
ONSA	–	0.86	0.85	0.82
ONS1	0.41	–	0.79	0.79
OTT5	0.44	0.50	–	0.79
OTT6	0.48	0.52	0.52	–
North gradient, GipsyX				
ONSA	–	0.87	0.92	0.90
ONS1	0.27	–	0.87	0.88
OTT5	0.21	0.27	–	0.91
OTT6	0.25	0.26	0.22	–
North gradient, c5++				
ONSA	–	0.78	0.79	0.75
ONS1	0.49	–	0.72	0.70
OTT5	0.46	0.55	–	0.74
OTT6	0.52	0.57	0.53	–

For the GipsyX results, the best agreement (the highest correlation and the lowest standard deviation) is seen between ONSA and OTT5, although the differences compared with OTT6 are small.

In order to investigate any dependence on the elevation cutoff angle we perform the same analysis using a cutoff angle equal to 20°. We chose 20° because it is comparable to the minimum elevation angle of the WVR observations, which gradients will be used for comparisons in the following subsections. These results are presented with the same layout in Table 5. The results show the same pattern. The ONS1 station has lower correlations, and higher standard deviations, when compared with the other stations. Of course, the geometry for estimating gradients is much worse, especially for the north gradient (see Fig. 3). This is, however, a common drawback for all four stations and we assume that the systematic errors introduced are similar for all stations which is a probable reason that the agreements are not much affected compared with the solution using a 5° elevation cutoff angle.

3.2. GPS vs WVR gradients with 5 min resolution

We now assess the GPS gradient results by a comparison with independent gradient estimates from the WVR. We use the time series with a 5 min temporal resolution

Table 5
Correlation coefficients (upper right triangle) and standard deviations in mm (lower left triangle) for gradient time series from the four GNSS stations using a 20° elevation cutoff angle.

Station	ONSA	ONS1	OTT5	OTT6
East gradient, GipsyX				
ONSA	–	0.87	0.95	0.94
ONS1	0.33	–	0.87	0.84
OTT5	0.20	0.33	–	0.96
OTT6	0.22	0.36	0.18	–
North gradient, GipsyX				
ONSA	–	0.82	0.91	0.90
ONS1	0.36	–	0.83	0.80
OTT5	0.26	0.36	–	0.92
OTT6	0.27	0.39	0.25	–

presented in the previous section and add also time series obtained using a 10° elevation cutoff angle. We ignore all data points that do not have a corresponding WVR gradient data point within ± 2 min.

The agreements between the WVR and the GipsyX solutions for the estimated total linear horizontal gradients are summarised in Table 6. We note the highest correlations and the lowest standard deviations are for the 5° cutoff angle at the two stations equipped with microwave absorbers (ONSA and OTT5). Again the differences compared with OTT6 are very small and slightly larger for ONS1. The 10° cutoff angle results are very close to those from the 5° solution. Obviously, too many GPS observations are ignored when an elevation cutoff angle of 20° is used. In spite of that the sampling of the atmosphere matches better with the WVR the agreements for the gradients are significantly worse.

Before continuing we point out that standard deviations, or the correlations, alone do not give the whole picture. For example, in Table 6 the correlations are higher in the east component, compared to the north component, but so are the standard deviations. If a time period does not have a lot of large gradients the correlation will be low, as well as the standard deviation, whereas a period with large gradients is likely to result in both higher correlations, as well as standard deviations. With this in mind it is interesting to use gradient data from periods when there are significant gradients only. Therefore we selected the data from time epochs when the total gradient amplitude from the WVR and ERA5 was larger than 2 mm and summarise the results in Table 7. Comparing these results to those obtained for all data in Table 6 we note that the correlations coefficients, as well as the standard deviations, increase significantly. But the relative differences between the four stations are very similar.

Another extreme subset of the data is to use periods when the WVR does not detect any large gradients. We selected all data from time epochs when the total gradient amplitude estimated from the WVR and ERA5 was less than 0.5 mm and summarise the results in Table 8.

In all the cases studied so far, we find that the best agreements are seen for the 5° elevation cutoff angle. Therefore, only these time series will be used in the following comparisons.

3.3. Gradients estimated with lower temporal resolutions

Another issue to address is the fact that the GPS gradients depend on the constraints used in the processing, resulting in correlations between adjacent estimated values. The WVR data are, however, based on 5 min of observations, where the 5 min gradient estimates are independent

Table 6
Agreement between the horizontal gradients from GipsyX and WVR gradients every 5 min.

Station	Correlation —		Standard deviation mm	
	East	North	East	North
5° GPS elevation cutoff angle, 38,122 data points				
ONSA	0.69	0.63	0.81	0.69
ONS1	0.66	0.59	0.84	0.71
OTT5	0.68	0.63	0.82	0.69
OTT6	0.68	0.62	0.82	0.69
10° GPS elevation cutoff angle, 37,866 data points				
ONSA	0.69	0.63	0.81	0.69
ONS1	0.66	0.57	0.84	0.73
OTT5	0.68	0.63	0.82	0.69
OTT6	0.68	0.61	0.82	0.70
20° GPS elevation cutoff angle, 38,122 data points				
ONSA	0.55	0.44	0.93	0.83
ONS1	0.53	0.37	0.94	0.87
OTT5	0.55	0.40	0.93	0.85
OTT6	0.54	0.41	0.93	0.84

Table 7
Agreement between the horizontal gradients from GipsyX and the WVR when the total gradients from the WVR > 2 mm, every 5 min.

Station	Correlation —		Standard deviation mm	
	East	North	East	North
5° GPS elevation cutoff angle, 4620 data points				
ONSA	0.77	0.74	1.58	1.32
ONS1	0.76	0.72	1.61	1.36
OTT5	0.77	0.73	1.60	1.33
OTT6	0.77	0.73	1.59	1.33
10° GPS elevation cutoff angle, 4613 data points				
ONSA	0.77	0.74	1.56	1.32
ONS1	0.75	0.68	1.60	1.40
OTT5	0.76	0.72	1.57	1.33
OTT6	0.77	0.72	1.57	1.35
20° GPS elevation cutoff angle, 4620 data points				
ONSA	0.69	0.59	1.73	1.51
ONS1	0.68	0.52	1.75	1.58
OTT5	0.68	0.57	1.74	1.53
OTT6	0.69	0.58	1.74	1.52

Table 8
Agreement between the horizontal gradients from GipsyX and the WVR when the total gradients from the WVR < 0.5 mm, every 5 min.

Station	Correlation —		Standard deviation mm	
	East	North	East	North
5° GPS elevation cutoff angle, 7833 data points				
ONSA	0.22	0.25	0.37	0.37
ONS1	0.20	0.25	0.40	0.38
OTT5	0.22	0.27	0.37	0.36
OTT6	0.22	0.26	0.38	0.37
10° GPS elevation cutoff angle, 7788 data points				
ONSA	0.20	0.26	0.39	0.38
ONS1	0.20	0.26	0.43	0.39
OTT5	0.21	0.26	0.40	0.37
OTT6	0.21	0.26	0.40	0.38
20° GPS elevation cutoff angle, 7833 data points				
ONSA	0.13	0.16	0.47	0.50
ONS1	0.14	0.15	0.50	0.53
OTT5	0.14	0.10	0.46	0.54
OTT6	0.12	0.13	0.48	0.52

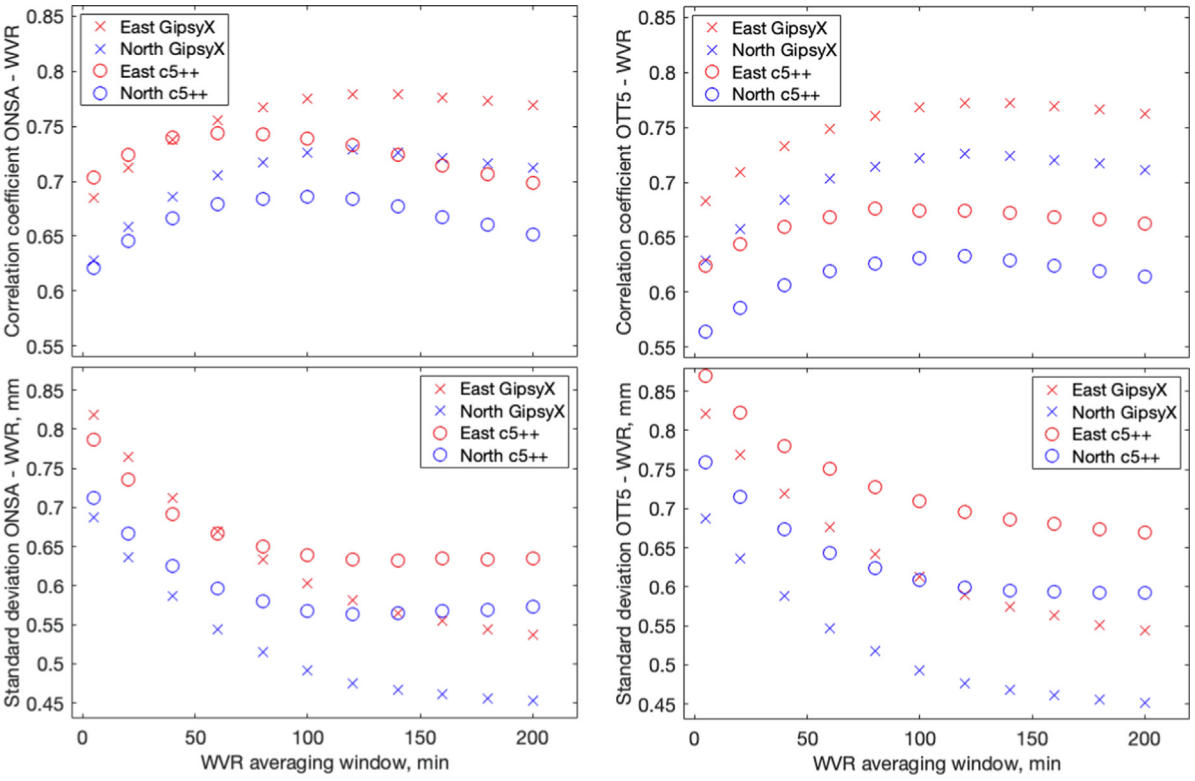

Fig. 6. Correlation coefficient (top) and standard deviation (bottom) between GPS based gradients and WVR gradients as a function of the averaging time applied to the WVR time series. The two stations with the best agreements for the non-averaged data are investigated, namely ONSA (left) and OTT5 (right).

from each other, i.e., there is no constraint from one estimated value to the next. This means that the estimated time series of gradients from the WVR show a much larger short term scatter compared to the ones from the GPS data. Therefore, we now apply different averaging times of the WVR gradients and compare them with those from the GipsyX and the c5++ processing. These results are shown in Fig. 6 for ONSA and OTT5.

We note that the correlation increases with averaging time and that the peaks occur for shorter averaging times when WVR gradients are compared with the gradients from c5++. We interpret this to be caused by the looser constraint applied in the c5++ processing. In the following we use 80 min and 120 min averages of the WVR gradients when compared with gradients from c5++ and GipsyX, respectively.

The effect of the smoothing the WVR gradients over a 120 min window, compared with the original 5 min data, is illustrated in Fig. 7. It depicts an example time series with relatively large gradients in the east component clearly detected by all four GNSS stations and the WVR. As expected the gradients from the GNSS stations still agree much better with each other compared to the WVR gradients. One question is to what extent the differences between the gradients from GNSS stations are significant and how they vary with time. This is addressed in the following subsections.

3.4. Gradients estimated month by month

As already discussed the results of gradient comparisons depend significantly on how many and how large gradients there are in the atmosphere during the studied time period. Therefore we investigated also the monthly results in terms of correlations and standard deviations. These are

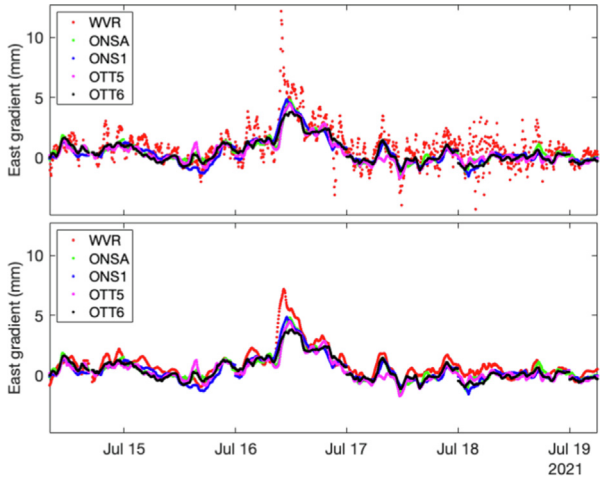

Fig. 7. Gradients in the east component estimated from the four GPS stations, processed with the GipsyX software, compared to the original (independent) WVR gradients (top) and WVR gradients averaged over a 120 min wide time window (bottom).

summarised in Fig. 8. The highest correlations are obtained during June (north gradient) and July (east gradient). This is as expected because there is more water vapour in the atmosphere, and it has a higher variability, during the summer months.

One of the largest differences for a station is seen for the north gradient estimated from the OTT5 data between the months of June and September. The reason is illustrated further in Fig. 9. We note that the higher correlation of the north gradients during June is due to larger gradients in general, and specifically one occasion with a negative gradient around −5 mm.

A detailed investigation revealed that there are significant large gradients, in both the east and the north components, during the last week of June. We chose to study these seven days as a special case.

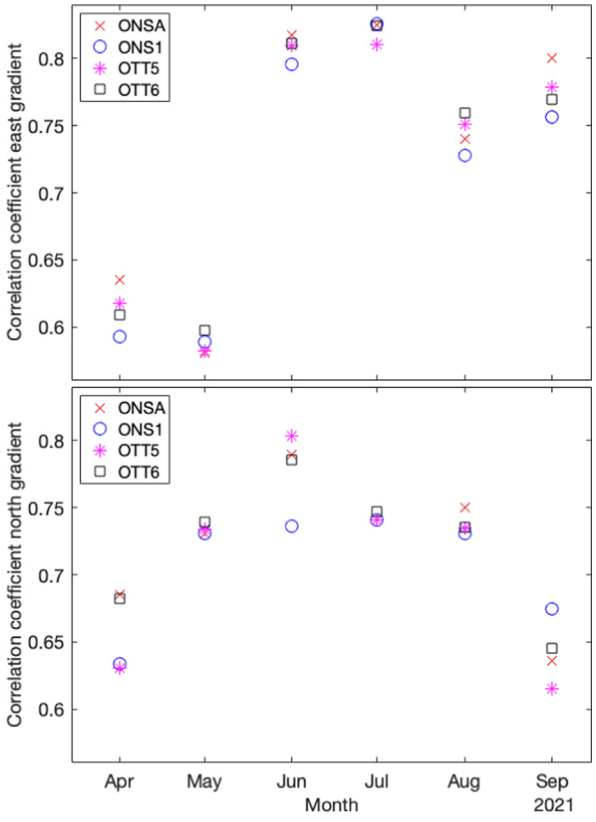

Fig. 8. Monthly correlation coefficients for the four stations between GPS based GipsyX processed east (top) and north (bottom) gradients and WVR gradients.

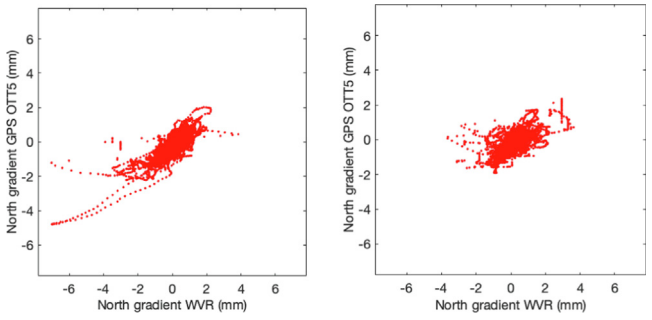

Fig. 9. North gradients from the OTT5 station for the months of June (left) and September (right). These are subsets of the data presented in Table 6. In June the correlation is 0.80 and the standard deviation is 0.48 mm. The corresponding values for September are 0.61 and 0.54 mm.

3.5. Case study: period with large gradients

The last seven days of June are selected for a comparison of the gradients estimated both from the GipsyX processing and the c5++ processing. It is motivated by the fact that c5++ gradients are estimated with a looser constraint which is an advantage in order to track rapid temporal variations in the gradients. The correlations and standard deviations are presented in Table 9. Again we note that the two stations equipped with absorbing material has overall a slightly better agreement with the WVR.

We examine the gradient time series for ONSA and ONS1 in Fig. 10 and Fig. 11, respectively. We chose these two stations because their gradients show the best and the worst agreement to the WVR gradients. In general the Gip-

Table 9
Comparison results for total linear horizontal gradients during 24–30 June 2021 for GPS observations processed with the GipsyX and the c5++ using a 5° elevation cutoff angle vs the corresponding WVR gradients.

Station	Correlation —		Standard deviation mm	
	East	North	East	North
GipsyX, WVR data 120 min average				
ONSA	0.83	0.87	0.53	0.54
ONS1	0.84	0.79	0.51	0.68
OTT5	0.86	0.88	0.48	0.53
OTT6	0.83	0.88	0.52	0.53
c5++, WVR data 80 min average				
ONSA	0.82	0.85	0.59	0.63
ONS1	0.73	0.77	0.69	0.78
OTT5	0.78	0.81	0.64	0.72
OTT6	0.76	0.76	0.67	0.81

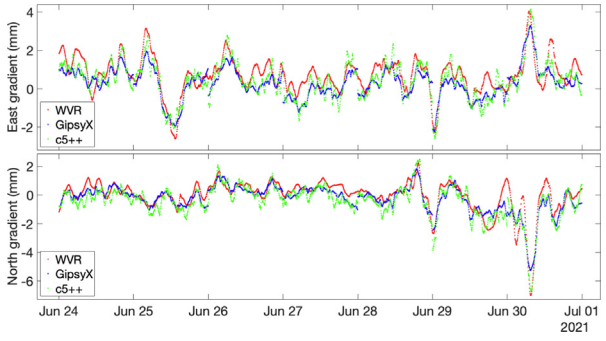

Fig. 10. Estimated east (top) and north (bottom) gradients using GipsyX (blue) and c5++ (green), a 5° elevation cutoff angle, and observations from the ONSA station. The corresponding correlations and standard deviations are found in Table 9. For simplicity only the WVR gradients (red) averaged over 120 min are shown in the graph.

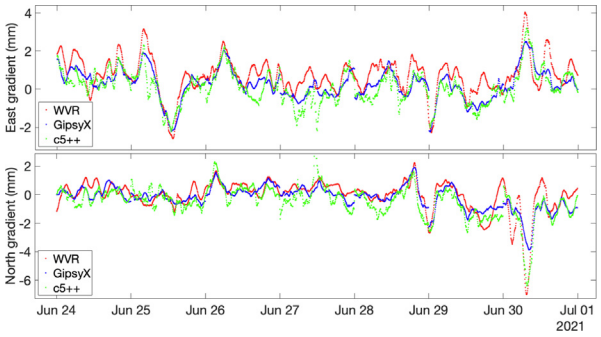

Fig. 11. Same as Fig. 10 but for the ONS1 station.

syX and c5++ follow the variations in the gradients observed by the WVR. We note that the looser constraint used in c5++ imply that rapid variations are more correctly detected, e.g. the large negative north gradient on 30 June. We also note that this occurs in spite of the sparse sampling (a sample period of 5 min) of the GPS observations. However, for an unknown reason the GipsyX processing of the ONS1 data does not track this negative gradient as well as it does using the ONSA data. This is one contribution to the lower correlation obtained for ONS1. The lower correlation obtained for the c5++ processing, on the other hand, is due to the larger scatter, especially on June 27 (see Figs. 10 and 11).

4. Discussion

We have compared four GNSS stations with different antenna installations. The overall agreements, for the whole six-month period, result in small differences between the four stations. For the geodetic application, monitoring station positions, the differences are not significant in terms of repeatability of daily estimation of station coordinates (and are therefore not presented or discussed further). But for meteorological applications, the rapid changes in gradients, or line of sight values, will be more important. If this is true also for multi-GNSS observations remains to be studied.

The fact that the agreements between the GPS gradients and the WVR gradients vary a lot from month to month is mainly a consequence of the size of the true gradients during each month. Another cause is varying environmental conditions. Multipath effects will change depending on nearby reflections, such as varying soil moisture in the ground or even the appearance of other nearby (unwanted) objects.

As pointed out by earlier studies, e.g., (Elgered et al., 2019), large gradients are typically associated with rapid changes in the ZWD. In order to track changes in the gradients in a more optimum way we may consider tuning the value of the constraint in the GPS data processing. A suggestion for future studies would hence be to use a constraint value that is tuned based on the ZWD variability. Of course this will require an iterative processing, first to obtain the ZWD variability and, thereafter, a second processing with an optimised constraint for the gradient estimations.

The geometry is important. One example is the slightly better agreement for the east gradient which we interpret to be caused by the inhomogeneous spatial sampling and is especially clear for the processing with the higher elevation cutoff angles, see Fig. 3 and Table 6. This is consistent with previous studies using data from the Onsala site (Elgered et al., 2019; Ning and Elgered, 2021).

The GNSS antenna installation OTT5, with a larger microwave absorber on the ground, is not significantly better than ONSA, which is also equipped with absorbing material, but has a much smaller area.

A drawback of this study was that only GPS satellites could be used in order to have a fair comparison of the stations. Using multi-GNSS and a higher elevation cutoff angle will make the GNSS and the WVR samples of the atmosphere more similar and will probably result in better agreements between the gradients from the WVR and all the GNSS stations (Ning and Elgered, 2021). With an improved agreement between the WVR and the GNSS gradients it will be easier to find differences in the quality of the stations.

5. Conclusions

We have presented some different methods to compare the quality of GNSS stations through the use of horizontal gradients in the atmosphere. First of all, because gradients vary a lot with time, it is important to use observations from the same time periods from the GNSS stations to be compared.

Initially the study was motivated to investigate if the non-standard antenna installation of OTT5 resulted in more accurate gradients. It is not possible to draw any such conclusion from this data set. The OTT5 station offers estimated gradients of comparable accuracy with the other stations. Instead the results were somewhat surprising in terms of identifying differences that we were not aware of. It is not clear if these are caused by varying multipath conditions or have another origin, e.g., different quality of the receivers. Such results are useful in future work in order to understand and improve the quality of the GNSS results.

The receivers at OTT5 and OTT6 were replaced as a consequence of this study. They now have better tracking of both Glonass and Galileo satellites and acquire multi-GNSS observations for future assessments of the stations.

Declaration of Competing Interest

The authors declare that they have no known competing financial interests or personal relationships that could have appeared to influence the work reported in this paper.

Acknowledgments

The geodetic research infrastructure at the Onsala Space Observatory is funded by Swedish Mapping, Cadastral and Land Registration Authority and Chalmers University of Technology.

References

Bar-Sever, Y.-E., Kroger, P.M., Börjesson, J.A., 1998. Estimating horizontal gradients of tropospheric path delay with a single GPS receiver. J. Geophys. Res. 103, 5019–5035. https://doi.org/10.1029/97jb03534.

Bertiger, W., Bar-Sever, Y., Dorsey, A., et al., 2020. GipsyX/RTGx, a new tool set for space geodetic operations and research. Adv. Space Res. 66, 469–489. https://doi.org/10.1016/j.asr.2020.04.015.

Boehm, J., Werl, B., Schuh, H., 2006. Troposphere mapping functions for GPS and very long baseline interferometry from European Centre for Medium-Range Weather Forecasts operational analysis data. J. Geophys. Res. 111, B02406. https://doi.org/10.1029/2005JB003629.

Chen, G., Herring, T., 1997. Effects of atmospheric azimuthal asymmetry on the analysis of space geodetic data. J. Geophys. Res. 102, 20489–20502. https://doi.org/10.1029/97JB01739.

Chen, B., Liu, Z., 2016. Global water vapor variability and trend from the latest 36 year (1979 to 2014) data of ECMWF and NCEP reanalyses, radiosonde, GPS, and microwave satellite. J. Geophys. Res. Atmos. 121, 11442–11462. https://doi.org/10.1002/2016JD024917.

Craig, R.A., Katz, I., Harney, P.J., 1945. Sea breeze cross sections from pyschrometric measurements. Bull. Am. Meteorol. Soc. 26 (10), 405–410. https://doi.org/10.1175/1520-0477-26.10.405.

Dach, R., Selmke, I., Villiger, A., Arnold, D., Prange, L., Schaer, S., Sidorov, D., Stebler, P., Jaäggi, A., Hugentobler, U., 2021. Review of recent GNSS modelling improvements based on CODEs Repro3 contribution. Adv. Space Res. 68 (3), 1263–1280. https://doi.org/10.1016/j.asr.2021.04.046.

Elgered, G., Ning, T., Forkman, P., Haas, R., 2019. On the information content in linear horizontal delay gradients estimated from space geodesy observations Atmos. Meas. Tech. 12, 3805–3823. https://doi.org/10.5194/amt-12-3805-2019.

Emardson, T.R., Johansson, J.M., Elgered, G., 2000. The systematic behavior of water vapor estimates using four years of GPS observations. Trans. IEEE Geosci. Remote Sens. 38, 324–329. https://doi.org/10.1109/36.823927.

Geremia-Nievinski, F., Hobiger, T., Haas, R., Liu, W., Strandberg, J., Tabibi, S., Vey, S., Wickert, J., Williams, S., 2020. SNR-based GNSS reflectometry for coastal sea-level altimetry: results from the first IAG inter-comparison campaign. J. Geod. 94, 70. https://doi.org/10.1007/s00190-020-01387-3.

Graffigna, V., Hernández-Pajares, M., Gende, M.A., Azpilicueta, F.J., Antico, P.L., 2019. Interpretation of the tropospheric gradients estimated with GPS during Hurricane Harvey. Earth Space Sci. 6, 1348–1365. https://doi.org/10.1029/2018EA000527.

Hobiger, T., Gotoh, T., Otsubo, T., Kubooka, T., Sekido, M., Takiguchi, H., Takeuchi, H., 2010 c5++ - Multi-technique analysis software for next generation geodetic instruments, IVS 2010 General Meeting Proceedings, pp. 212–216, https://ivscc.gsfc.nasa.gov/publications/gm2010/hobiger2.pdf.

Kačmařík, M., Douša, J., Zus, F., Václavovic, P., Balidakis, K., Dick, G., Wickert, J., 2019. Sensitivity of GNSS tropospheric gradients to processing options. Ann. Geophys. 37, 429–446. https://doi.org/10.5194/angeo-37-429-2019.

Kierulf, H.P., Steffen, H., Barletta, V.R., Lidberg, M., Johansson, J., Kristiansen, O., Tarasov, L., 2021. A GNSS velocity field for geophysical applications in Fennoscandia. J. Geodyn. 146, 101845. https://doi.org/10.1016/j.jog.2021.101845.

Kuettner, J.P., 1971. Cloud bands in the earth's atmosphere: observations and theory. Tellus 23 (4–5), 404–426. https://doi.org/10.3402/tellusa.v23i4-5.10519.

Landskron, D., Bohm, J., 2018. VMF3/GPT3: refined discrete and empirical troposphere mapping functions. J. Geod. 92, 349–360. https://doi.org/10.1007/s00190-017-1066-2.

Lidberg, M., Johansson, J.M., Scherneck, H.-G., Milne, G.A., 2010. Recent results based upon continuous GPS Observations of the GIA process in Fennoscandia from BIFROST. J. Geodyn. 50, 8–18. https://doi.org/10.1016/j.jog.2009.11.010.

Lindskog, M., Ridal, M., Thorsteinsson, S., Ning, T., 2017. Data assimilation of GNSS zenith total delays from a Nordic processing centre. Atmos. Chem. Phys. 17, 13983–13998. https://doi.org/10.5194/acp-17-13983-2017.

Lyard, F., Lefevre, F., Letellier, T., Francis, O., 2006. Modelling the global ocean tides: Modern insights from FES2004. Ocean Dyn. 56, 394. https://doi.org/10.1007/s10236-006-0086-x.

Matteo, N.A., Morton, Y.T., 2011. Ionosphere geomagnetic field: Comparison of IGRF model prediction and satellite measurements 1991–2010. Radio Sci. 46. https://doi.org/10.1029/2010RS004529, RS4003.

Miller, S.T.K., Keim, B.D., Talbot, R.W., Mao, H., 2003. Sea breeze: Structure, forecasting, and impacts. Rev. Geophys. 41 (3), 1011. https://doi.org/10.1029/2003RG000124.

Morel, L., Pottiaux, E., Durand, F., Fund, F., Boniface, K., de Oliveira, P.S., Van Baelen, J., 2015. Validity and behaviour of tropospheric gradients estimated by GPS in Corsica, Adv. Space Res. 55, 135–149. https://doi.org/10.1016/j.asr.2014.10.004.

Ning, T., Elgered, G., 2021. High-temporal-resolution wet delay gradients estimated from multi-GNSS and microwave radiometer observations Atmos. Meas. Tech. 14, 5593–5605. https://doi.org/10.5194/amt-14-5593-2021.

Ning, T., Elgered, G., Johansson, J.M., 2011. The impact of microwave absorber and radome geometries on GNSS measurements of station coordinates and atmospheric water vapour. Adv. Space. Res. 47 (2), 186–196. https://doi.org/10.1016/j.asr.2010.06.023.

Parracho, A.C., Bock, O., Bastin, S., 2018. Global IWV trends and variability in atmospheric reanalyses and GPS observations. Atmos. Chem. Phys. 18, 16213–16237. https://doi.org/10.5194/acp-18-16213-2018.

Petovello, M.G., O'Keefe, K., Lachapelle, G., Cannon, M.E., 2009. Consideration of time-correlated errors in a Kalman filter applicable to GNSS. J. Geod. 83, 51–56. https://doi.org/10.1007/s00190-008-0231-z.

Schmid, R., Steigenberger, P., Gendt, G., Ge, M., Rothacher, M., 2007. Generation of a consistent absolute phase center correction model for GPS receiver and satellite antennas. J. Geod. 81, 781–798. https://doi.org/10.1007/s00190-007-0148-y.

Schmid, L., Koch, F., Heilig, A., Prasch, M., Eisen, O., Mauser, W., Schweizer, J., 2015. A novel sensor combination (upGPR-GPS) to continuously and nondestructively derive snow cover properties. Geophys. Res. Lett. 42, 3397–3405. https://doi.org/10.1002/2015GL063732.

re3data.org: VMF Data Server; editing status 2020–12-14; re3data.org - Registry of Research Data Repositories, https://doi.org/10.17616/R3RD2H.

Westwater, E.R., Guiraud, F.O., 1980. Ground-based microwave radiometric retrieval of precipitable water vapor in presence of clouds with high liquid content. Radio Sci. 15, 947–957. https://doi.org/10.1029/RS015i005p00947.

Zus, F., Deng, Z., Wickert, J., 2017. The impact of higher-order ionospheric effects on estimated tropospheric parameters in Precise Point Positioning. Radio Sci. 52, 963–971. https://doi.org/10.1002/2017RS006254.

Zus, F., Douša, J., Kačmařík, M., Václavovic, P., Dick, G., Wickert, J., 2019. Estimating the impact of global navigation satellite system horizontal delay gradients in variational data assimilation. Remote Sens. 11 (1), 41. https://doi.org/10.3390/rs11010041.